BIOCHEMISTRY
including biophysical chemistry & molecular biology

ARTICLE

pubs.acs.org/biochemistry

Targeting the Role of a Key Conserved Motif for Substrate Selection and Catalysis by 3-Deoxy-D-*manno*-octulosonate 8-Phosphate Synthase

Timothy M. Allison,[‡] Richard D. Hutton,[‡] Fiona C. Cochrane,[†] Jeffrey A. Yeoman,[†] Geoffrey B. Jameson,[†] and Emily J. Parker*[,‡]

[†]The Riddet Institute and Institute of Fundamental Sciences, Massey University, Palmerston North, New Zealand

[‡]Biomolecular Interaction Centre and Department of Chemistry, University of Canterbury, Christchurch, New Zealand

Supporting Information

ABSTRACT: 3-Deoxy-D-*manno*-octulosonate 8-phosphate synthase (KDO8PS) catalyzes the reaction between three-carbon phosphoenolpyruvate (PEP) and five-carbon D-arabinose 5-phosphate (A5P), generating KDO8P, a key intermediate in the biosynthetic pathway to 3-deoxy-D-*manno*-octulosonate, a component of the lipopolysaccharide of the Gram-negative bacterial cell wall. Both metal-dependent and metal-independent forms of KDO8PS have been characterized. KDO8PS is evolutionarily and mechanistically related to the first enzyme of the shikimate pathway, the obligately divalent metal ion-dependent 3-deoxy-D-*arabino*-heptulosonate 7-phosphate synthase (DAH7PS) that couples PEP and four-carbon D-erythrose 4-phosphate (E4P) to give DAH7P. In KDO8PS, an absolutely conserved KANRS motif forms part of the A5P binding site, whereas in DAH7PS, an absolutely conserved KPR(S/T) motif accommodates E4P. Here, we have characterized four mutants of this motif (AANRS, KAARS, KARS, and KPRS) in metal-dependent KDO8PS from *Acidithiobacillus ferrooxidans* and metal-independent KDO8PS from *Neisseria meningitidis* to test the roles of the universal Lys and the Ala-Asn portion of the KANRS motif. The X-ray structures, determined for the *N. meningitidis* KDO8PS mutants, indicated no gross structural penalty resulting from mutation, but the subtle changes observed in the active sites of these mutant proteins correlated with their altered catalytic function. (1) The AANRS mutations destroyed catalytic activity. (2) The KAARS mutations lowered substrate selectivity, as well as activity. (3) Replacing KANRS with KARS or KPRS destroyed KDO8PS activity but did not produce a functional DAH7PS. Thus, Lys is critical to catalysis, and other changes are necessary to switch substrate specificity for both the metal-independent and metal-dependent forms of these enzymes.

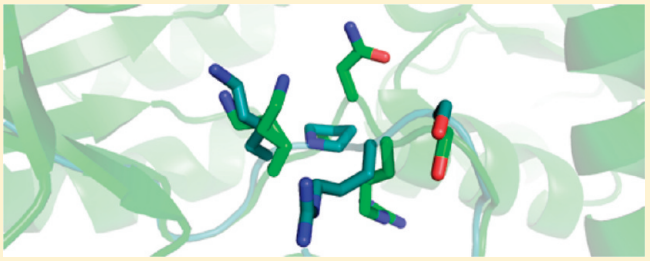

The enzyme 3-deoxy-D-*manno*-octulosonate 8-phosphate (KDO8P) synthase (EC 2.5.1.55) catalyzes the aldol-like reaction between D-arabinose 5-phosphate (A5P) and phosphoenolpyruvate (PEP), producing KDO8P (Figure 1).[1] KDO8P is subsequently dephosphorylated to form 3-deoxy-D-*manno*-octulosonate (KDO), an essential component in the lipopolysaccharide (LPS) layer in the cell wall of Gram-negative bacteria.[2] The enzymes responsible for KDO biosynthesis have been identified as potential targets for antibacterial drug design.[3] KDO8P synthase is mechanistically and evolutionarily related to 3-deoxy-D-*arabino*-heptulosonate 7-phosphate (DAH7P) synthase (EC 2.5.1.54), the enzyme that catalyzes the first step of the shikimate pathway for the biosynthesis of aromatic compounds in plants and microorganisms.[4] DAH7P synthase catalyzes a reaction in which the four-carbon D-erythrose 4-phosphate (E4P) rather than the five-carbon A5P is coupled with PEP.

Structures of KDO8P synthases and DAH7P synthases from a variety of sources have been determined, and these proteins have been shown to share a similar $(\beta/\alpha)_8$ TIM-barrel monomeric unit.[5−14] For KDO8P synthases examined to date, these monomer units have been shown to assemble into similar tetramers. In contrast, the overall structures of the DAH7P synthases are more variable, with barrel extensions and quaternary structure variations associated with allosteric regulation by aromatic end products.[7,15−17] DAH7P synthases have been divided into a number of families, and KDO8P synthases appear to be most closely related to the type Iβ group of DAH7P synthases. These proteins share the highest level of sequence identity (~30%) with KDO8P synthase and have been shown to adopt a similar tetrameric quaternary structure.[18−20]

There are two distinct types of KDO8P synthases that differ in their requirement for a divalent metal ion for catalytic activity.[19,21,22] In metal-dependent enzymes, the side chains of four active-site residues, Cys, Asp, Glu, and His, coordinate to the

Received: February 18, 2011
Revised: March 21, 2011
Published: March 25, 2011

metal ion. These residues are conserved in both metal-dependent and metal-independent enzymes, apart from the Cys, where in metal-independent enzymes this is replaced with an invariant Asn. Although a metal-dependent KDO8PS can be converted to a metal-independent mutant, and vice versa, by Cys-to-Asn or Asn-to-Cys substitution, for optimal activity these changes must be coupled with other mutations on nearby loops.[10,22−26] The role of the metal ion seems to be structural rather than directly catalytic, to organize and position the active-site residues and particularly the A5P substrate.[27] This role appears to be equivalently played by the amide side chain of the invariant Asn at the Cys/Asn site. In marked contrast to the KDO8P synthases, all DAH7P synthases characterized so far require a divalent metal ion for activity, and accordingly, all four metal-binding residues are conserved.[28] For DAH7P synthase, the metal ion may play a more critical role in enzymic function. It has been proposed that KDO8P synthase and DAH7P synthase coevolved from a common ancestral metal-dependent DAH7P synthase. Subsequently, metal dependency was discarded for some KDO8P synthases.[19,29]

Many of the key details of the reactions catalyzed by both KDO8P synthase and DAH7P synthase have been elucidated. It is known that the *si* face of PEP attacks the *re* face of the A5P or E4P aldehydic cosubstrate.[30] This is followed by the attack of water, forming a linear tetrahedral intermediate, from which the phosphate ester of the PEP parent is subsequently eliminated through cleavage of the C−O bond.[27,31] However, what is less clear is how specific substrate selection is controlled by these enzymes. DAH7P synthases have been shown to be relatively promiscuous and utilize, with variable efficiency, A5P and other five-carbon aldehyde substrates, as well as E4P and its derivatives, such as 2-deoxyE4P.[28,32] On the other hand, KDO8P synthases exhibit tight specificity: the enzyme is not just specific to carbon length but also does not tolerate diastereoisomeric substrates in which the configurations of the hydroxyl groups at positions 2 and/or 3 are inverted.[33,34]

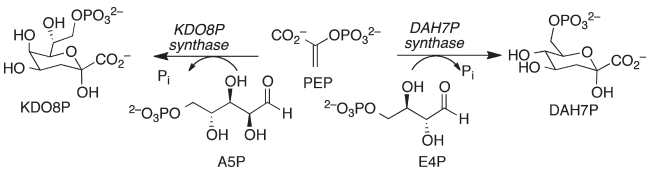

Figure 1. Reactions catalyzed by KDO8P and DAH7P synthases.

Many of the residues that directly contact substrates are invariant for all KDO8P and DAH7P synthases. However, of particular note to substrate selection is an absolutely conserved motif of five amino acids in KDO8P synthases that has been shown to interact directly with A5P. This Lys-Ala-Asn-Arg-Ser (KANRS) motif is present on the $\beta_2\alpha_2$ loop of the $(\beta/\alpha)_8$ barrel and is an integral part of the enzyme active site. In structures of KDO8P synthase from the hyperthermophile *Aquifex aeolicus* (*Aae*KDO8PS), in which both PEP and A5P are bound, this motif is responsible for the key interactions of the enzyme with A5P (Figure 2).[12,25] The Arg and Ser residues coordinate to the phosphate moiety of A5P and form the phosphate-binding site for the aldose substrate, along with an Arg contributed by the adjacent subunit, and a Ser from the $\beta_7\alpha_7$ loop. The Asn residue of this KANRS motif forms hydrogen bonds to the C2 and C4 hydroxyl groups of A5P, providing contacts that may help to orient the reactive carbonyl of A5P in the active site. The Lys is positioned close to the A5P carbonyl and potentially may play a role in its activation.[25] In DAH7P synthases, an absolutely conserved Lys-Pro-Arg-Ser/Thr (KPRS) motif occupies the same position as the KANRS motif of the KDO8P synthases and is responsible for the interactions between the enzyme and substrate E4P. It is likely that this obvious conserved difference plays an important role in determining the differential substrate selection of the two enzymes.

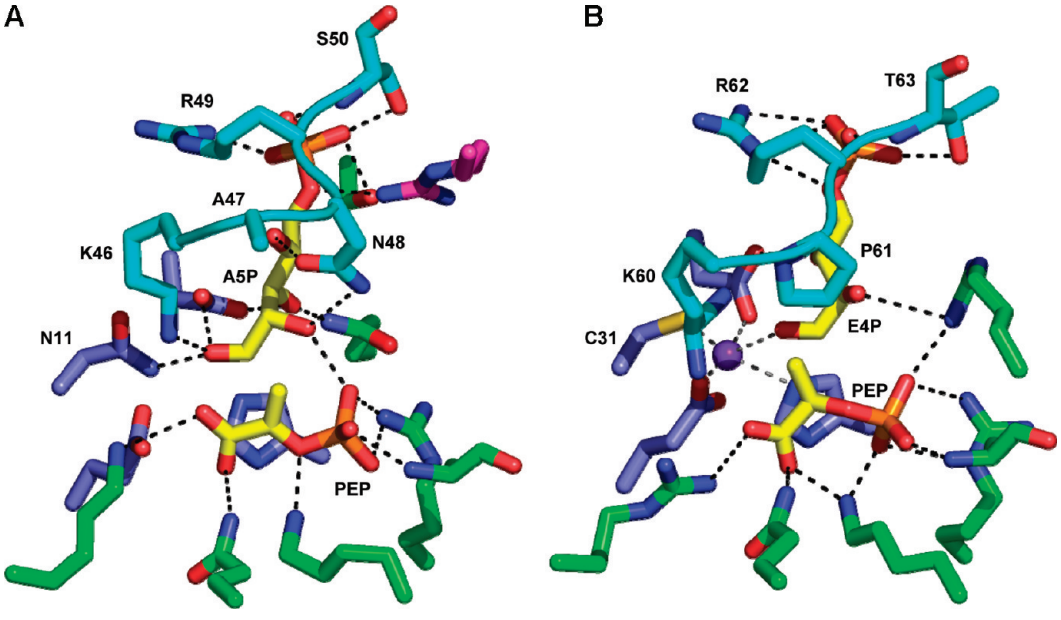

Figure 2. Binding of A5P and E4P to the active site of KDO8P synthase and DAH7P synthase. (A) *Aae*KDO8PS C11N/S235P/Q237A mutant, PDB entry 2NX3,[25] chain B. (B) *Pyrococcus furiosus* DAH7PS, PDB entry 1ZCO, E4P shown as modeled by Schofield et al.[9] The carbon atoms of the KANRS and KPRT motifs are colored cyan, those of the metal-binding site residues blue, those of the PEP-binding residues green, those of residues from an adjacent subunit magenta, and those of PEP and A5P yellow. The manganese ion in panel B is colored purple.

In this study, we have examined the importance of the KANRS motif for catalysis and substrate selection by a metal-dependent and -independent KDO8P synthase. These studies disclose an essential catalytic role for the Lys of this motif and also illustrate the importance of the Asn in substrate selection.

EXPERIMENTAL PROCEDURES

Bacterial Strains, Plasmids, Media, and Growth Conditions. The wild-type and mutant proteins were expressed with methods similar to those described previously.[10,26] Briefly, *Escherichia coli* BL21(DE3) (Star) cells carrying plasmids encoding the genes for each protein under control of a T7 promoter were grown to an OD_{600} of 0.4−0.8 at 37 °C. At this point, expression was induced via addition of IPTG to a final concentration of 0.5 or 1 mM. Cells were harvested 4 h postinduction or were immediately cooled after induction to 23 °C and harvested the following morning (~16 h).

Site-Directed Mutagenesis. Mutants of the plasmid containing the gene for *Afe*KDO8PS and that containing the gene for *Nme*KDO8PS were generated using a QuikChange II Site-Directed Mutagenesis Kit (Stratagene) or a Quikchange II Lightning Site-Directed Mutagenesis Kit (Stratagene). Using the pT7-7-*Afe*KDO8PS plasmid as the template, K55A, N57A, N57D, and N57del (KARS) mutant DNA was generated using the following primers: K55A, 5′-GTTCCTACGATGCAGCGAACCGTTCTTCG (forward) and 5′-CGAAGAACGGTTCGCTGCATCGTAGGAAC (reverse); N57A, 5′-CCTACGATAAAGCGGCACGTTCTTCGGGGCAG (forward) and 5′-CTGCCCCGAAGAACGTGCCGCTTTATCGTAGG (reverse); N57D, 5′-CTACGATAAAGCGGACCGTTCTTCGGG (forward) and 5′-CCCGAAGAACGGTCCGCTTTATCGTAG (reverse); N57del, 5′-CTACGATAAAGCG***CGTTCTTCGGGGC (forward) and 5′-GCCCCGAAGAACG***CGCTTTATCGTAG (reverse). Using the N57del plasmid as a template, A56P/N57del (KPRS) was created using the following primers: forward, 5′-GTTCCTACGATAAACCGCGTTCTTCGGGGC; reverse, 5′-GCCCCGAAGAACGCGGTTTATCGTAGGAAC. The mutants of *Nme*KDO8PS were generated using the same methods with the following primers: K57A, 5′-CTTTAAAGCCTCTTTCGACGCGGCAAACCGTTC (forward) and 5′-GAACGGTTTGCCGCGTCGAAAGAGGCTTTAAAG (reverse); N59A, 5′-CTCTTTCGACAAGGCAGCACGTTCCTCCATCCATTC (forward) and 5′-GAATGGATGGAGGAACGTGCTGCCTTGTCGAAAGAG (reverse); N59D, 5′-CTTTCGACAAGGCAGACCGTTCCTCCATC (forward) and 5′-GATGGAGGAACGGTCTGCCTTGTCGAAAG (reverse); N59del, 5′-CTTTCGACAAGGCA***CGTTCCTCCATCC (forward) and 5′-GGATGGAGGAACG***TGCCTTGTCGAAAG (reverse); A58P, 5′-CCTCTTTCGACAAGCCGCGTTCCTCCATCC (forward) and 5′-GGATGGAGGAACGCGGCTTGTCGAAAGAGG (reverse).

PCR products were transformed into competent *E. coli* XL1-Blue or *E. coli* TOP-10 cells. Plasmids were extracted from several transformant colonies and sequenced, confirming successful site-directed mutagenesis after which plasmids were further transformed into competent *E. coli* BL21(DE3) (Star) cells for protein overexpression.

Enzyme Purification and Assays. All enzymes were purified as previously described using anion exchange and hydrophobic interaction chromatography, followed by size exclusion chromatography.[10,26] The kinetic assay system used was the same as that previously described, based on the rate of consumption of PEP ($\varepsilon = 2.8 \times 10^3\ M^{-1}\ cm^{-1}$) measured by the loss of absorbance at 232 nm.

Differential Scanning Fluorimetry. The melting temperatures of wild-type and mutant *Afe*KDO8PS and *Nme*KDO8PS were determined by differential scanning fluorimetry using an iCycler iQ5Multicolour Real-Time PCR Detection System (Bio-Rad). The method used was based on that of Nordlund et al.[35] Triplicate protein samples were added with mixing to buffer (containing additives) and SYPRO orange dye in a 96-well microplate, which was then sealed. The melt proceeded in 0.2 °C increments from 20 to 95 °C, with a 20 s dwell time after each temperature increase. Measurements of the fluorescence were taken at the end of each dwell time. The melt temperatures were calculated as the temperature of maximal inflection of the melting curve after subtraction of the reading of a blank well containing buffer and dye but lacking protein.

Michaelis−Menten Kinetics. The assays for determining the kinetic parameters contained 10 mM BTP (pH 7.5), a variable amount of PEP and A5P, and, for mutants of *Afe*KDO8PS, 100 μM $MnSO_4$. For each enzyme, the following concentrations of substrates were used: 100 μM PEP and 88.5−3540 μM A5P for *Nme*N59A, 788 μM A5P and 4.97−99.4 μM PEP for *Nme*N59A, 100 μM PEP and 210−7965 μM A5P for *Nme*KARS, 800 μM A5P and 10−100 μM PEP for *Nme*KARS, 115 μM PEP and 15.75−525 μM A5P for *Nme*KPRS, 158 μM A5P and 4.97−99.4 μM PEP for *Nme*KPRS, 100 μM PEP and 27.6−345 μM A5P for *Afe*N57A, and 800 μM A5P and 1.95−26.0 μM PEP for *Afe*N57A. Substrate concentrations of up to 200 μM PEP and 1 mM A5P were used to test for activity of those mutants with no perceptible activity.

Substrate Specificity. Substrate specificity was assessed using the standard assay, using 200 μM PEP, and up to 1 mM alternate aldose substrate. The substrate concentrations for determining the kinetic parameters of 2-deoxyR5P with *Nme*N59A were 100 μM PEP and 86.6−1732 μM 2-deoxyR5P and for *Afe*N57A 100 μM PEP and 78−3900 μM 2-deoxyR5P.

Isothermal Titration Calorimetry. The binding of *Nme*K57A and *Afe*K55A to PEP was assessed by isothermal titration calorimetry, using a VP-ITC unit operating at 298 K (Microcal, GE Healthcare). Protein was buffer-exchanged against binding buffer, and all solutions were degassed in a vacuum before being used. The binding buffer for *Nme*K57A was 50 mM BTP (pH 7.0), and titrations comprised 29 injections of ligand, one 2 μL injection followed by twenty-eight 10 μL injections. The syringe concentration of PEP was 650 μM, and the concentration of *Nme*K57A in the cell was 50 μM. The buffer used for *Afe*K55A was the same but with the addition of 0.5 mM $MnSO_4$, and the injection protocol was also the same. The PEP concentration in the syringe was 1.5 mM, and the *Afe*K55A concentration in the cell was 150 μM. To allow for diffusion of the ligand across the needle tip during the equilibration period, the initial data point was routinely deleted. Heats of dilution experiments were measured independently and subtracted from the integrated data before curve fitting in Origin 7.0 with the standard one-site model supplied by MicroCal.

Crystallization. Crystals of *Nme*K57A, *Nme*N59A, *Nme*KARS, and *Nme*KPRS were grown by hanging drop vapor diffusion. A protein solution [20 mg/mL, in 10 mM BTP (pH 7.5)] of each mutant was mixed 1:1 (v/v) with a reservoir solution containing 100 mM sodium acetate (pH 4.6) and 0.6−3.0 M NaCl. The drop sizes were 2 μL, and the volume of reservoir solution was 500 μL. The crystallization trays were left at 20 °C until immediately before data collection, with crystals being transferred briefly into a cryoprotectant composed of 20% glycerol in the respective

Table 1. Crystal Parameters, Data Collection, and Refinement Statistics

	*Nme*K57A	*Nme*N59A	*Nme*KARS	*Nme*KPRS
		Data Collection		
crystal system, space group	orthorhombic, $P2_12_12_1$	orthorhombic, $P2_12_12_1$	orthorhombic, $P2_12_12_1$	orthorhombic, $P2_12_12_1$
unit cell parameters *a*, *b*, *c* (Å)	82.43, 86.18, 163.31	81.64, 85.37, 162.62	82.03, 85.81, 163.14	81.82, 85.15, 163.78
resolution range (Å)	34.59−1.95 (2.02−1.95)	39.93−1.75 (1.81−1.75)	36.84−1.90 (1.97−1.90)	55.47−2.70 (2.85−2.70)
no. of measurements	431450	424611	412547	150576
no. of unique reflections	83787	106837	91249	32102
redundancy	5.15 (5.16)	3.97 (2.98)	4.52 (4.36)	4.7 (4.80)
completeness (%)	98.0 (100)	92.8 (65.2)	99.4 (97.3)	99.7 (99.5)
$I/\sigma(I)$	4.2 (1.6)	8.8 (1.9)	5.1 (2.1)	5.9 (1.5)
R_{merge}	0.079 (0.394)	0.036 (0.355)	0.070 (0.357)	0.119 (0.503)
Wilson *B* value (Å^2)	33.8	34.1	26.5	45.8
		Refinement		
resolution (Å)	33.84−1.95 (2.00−1.95)	40.00−1.75 (1.80−1.75)	36.66−1.90 (1.95−1.90)	47.89−2.70 (2.77−2.70)
R_{cryst}	0.2048	0.1800	0.1887	0.2112
R_{free}	0.2521	0.2152	0.2285	0.2749
amino acids (chain length of 280 residues)	250 + 250 + 251 + 249 residues; 7827 atom sites	251 + 252 + 252 + 254 residues; 7828 atom sites	243 + 247 + 249 + 240 residues; 7532 atom sites	249 + 251 + 249 + 251 residues; 7711 atom sites
no. of water molecules	737	698	717	139
no. of others	3 (1 × 0.5) Cl^-, 1 Na^+, 1 glycerol	8 Cl^-, 1 Na^+, 0.5 PO_4^{2-}, 2 (1 × 0.5) glycerol	4 Cl^-, 2 Na^+, 2 glycerol	none
mean *B* (Å^2)				
protein	36.44	31.53	28.19	34.35
water	43.43	39.85	36.60	32.77
other	25.44	38.75	30.75	–
rmsd from target values				
bond lengths (Å)	0.010	0.010	0.008	0.008
bond angles (deg)	1.090	1.201	0.932	1.115
dihedral angles (deg)	6.623	5.402	6.437	5.082
Ramachandran				
most favored (%)	92.4	93.5	92.6	93.2
allowed (%)	6.6	5.5	6.2	5.7
generously allowed (%)	0.6	0.7	0.6	0.6
disallowed (%)	0.5	0.3	0.6	0.5
PDB entry	3QPY	3QPZ	3QQ0	3QQ1

reservoir solution. Crystals typically began to form after 4 h and were fully formed in 24 h.

Determination and Refinement of Structure. A Rigaku MicroMax007 microfocus copper rotating-anode generator with AXCo PX70 focusing capillary optics (λ = 1.5418 Å) coupled with an RAxisIV^{++} image plate detector was used to collect data sets at 120 K (Oxford Cryosystems Series 700) for *Nme*K57A, *Nme*N59A, and *Nme*KARS. Data collection and processing were performed with CrystalClear.[36]

Data sets for *Nme*KPRS were collected at the Australian Synchrotron using the Micro Crystallography (MX2) beamline and were processed using iMosFlm version 1.0.4 and SCALA (CCP4 suite[37]). The results are summarized in Table 1, along with key structure refinement details. Data were collected from crystals of *Nme*K57A grown in 2.2 M NaCl, *Nme*N59A grown in 1.0 M NaCl, *Nme*KARS grown in 1.4 M NaCl, and *Nme*KPRS grown in 2.6 M NaCl. All four mutant proteins crystallize like the wild type in orthorhombic space group $P2_12_12_1$ and diffracted to 1.95, 1.75, 1.90, and 2.70 Å, respectively, with the following unit cell dimensions: $a \approx 82$ Å, $b \approx 85$ Å, and $c \approx 163$ Å. The wild-type *Nme*KDO8PS structure was used to determine the structure of the three mutants, carrying through the same set of reflections for calculation of R_{free}. Refinements were conducted with Refmac5,[38] and electron density maps were analyzed with COOT.[39] The validation tools of COOT were used to check for, and correct, conformational infelicities. All diagrams were drawn with PyMol.

RESULTS

Preparation of A5P Binding-Site Mutants. The KANRS motif, located in the A5P binding site, is absolutely conserved across all known KDO8P synthases. To examine the role of this motif, we employed both a metal-dependent form (from *Acidithiobacillus ferrooxidans*, *Afe*KDO8PS) and a metal-independent form (from *Neisseria meningitidis*, *Nme*KDO8PS). A sequence alignment is provided in Figure S1 of the Supporting Information.

Table 2. Kinetic Parameters for Wild-Type and Mutant *Nme*KDO8PS and *Afe*KDO8PS Enzymes

	K_m^{PEP} (μM)	K_m^{A5P} (μM)	k_{cat} (s^{-1})[a]	k_{cat}/K_m^{A5P} (s^{-1} mM^{-1})
wild-type *Nme*	2.5 ± 0.2	12.0 ± 0.5	8.0 ± 0.1	660 ± 40
*Nme*K57A	–	–	–	
*Nme*N59A	7.9 ± 0.7	503 ± 28	0.149 ± 0.002	0.29 ± 0.02
*Nme*N59D	–	–	–	
*Nme*KARS	43 ± 11	1100 ± 200	0.0178 ± 0.0007	0.016 ± 0.004
*Nme*KPRS	–	–	–	
wild-type *Afe*	12 ± 1	22 ± 2	4.8 ± 0.1	220 ± 20
*Afe*K55A	–	–	–	
*Afe*N57A	2.9 ± 0.6	81 ± 4	0.30 ± 0.01	3.7 ± 0.3
*Afe*N57D	–	–	–	
*Afe*KARS	–	–	–	
*Afe*KPRS	–	–	–	

[a] Enzymes for which no activity was measurable (k_{cat} < 0.001 s^{-1}) are denoted with dashes.

The Lys residue of this motif is conserved in both the KDO8P synthases and the related DAH7P synthases. It has been proposed that the amino moiety of this residue plays a role in the protonation of the A5P carbonyl functionality in catalysis for KDO8P synthases.[25] We generated mutant proteins of both *Afe*KDO8PS and *Nme*KDO8PS from which this functionality had been removed (K55A and K57A in *Afe*KDO8PS and *Nme*KDO8PS, respectively).

The adjacent Ala and Asn residues represent the conserved difference between KDO8P synthases and DAH7P synthases, and these residues are likely to play a role in determining substrate selection. We produced mutants in which the amide functionality of the Asn was removed (N57A and N59A) and or altered to a carboxylate moiety (N57D and N59D) to ascertain whether an isosteric hydrogen bond acceptor would suffice in this position. In addition, we created deletion mutants by removing this Asn residue and substituted both Ala and Asn with Pro, thereby creating the conserved KPRS motif of the DAH7P synthases.

Mutant proteins were purified according to procedures developed for the respective wild-type proteins. The masses of the purified proteins were confirmed by liquid chromatography and mass spectrometry, and the structural integrity for the mutants of *Afe*KDO8PS was assessed by circular dichroism spectrophotometry (Table S1 and Figure S2 of the Supporting Information).

The melting temperatures of *Afe*KDO8PS and *Nme*KDO8PS mutant proteins were determined by differential scanning fluorimetry and were similar to those previously measured for the respective wild-type proteins (Table S2 of the Supporting Information). *Nme*KARS and *Nme*KPRS mutants both have overall lower melting temperatures, indicating that these mutations affect the inherent stability of the enzyme.

Mutations in the A5P Binding Site Alter the Kinetic Profile of KDO8PS. The catalytic activities of all mutants were assessed (Table 2). Mutation of the KANRS motif Lys was completely deleterious to enzyme function, with both *Nme*K57A and *Afe*K55A having no perceptible activity. Compromised catalytic activity was observed for the mutants in which the Asn residue was altered to Ala. In accord with the importance of this residue for A5P binding, A5P K_m was significantly increased, whereas the K_m values with respect to PEP were only slightly increased. However, the substitution of the amide moiety of this Asn by the carboxylate functionality did not produce functional enzymes. Contraction of the KANRS motif and its alteration to the DAH7PS-like KPRS motif also rendered inactive enzymes. The *Nme*KARS mutant was the only exception to this; however, its maximal rate of reaction was more than 400 times slower than that observed for the wild-type enzyme, and the K_m values determined for this enzyme, particularly for the use of A5P, were significantly higher than those observed for the wild-type enzyme.

Wild-type enzymes and mutants were also tested for their ability to accept alternative aldose phosphates as substrates to A5P (Table 3). None of the enzymes exhibited any activity with E4P, the natural substrate of the related enzyme DAH7P synthase. Ribose 5-phosphate was similarly not accepted as an alternative. However, both wild-type enzymes and the compromised Asn mutants (*Nme*N59A and *Afe*N57A) were both able to accept 2-deoxyribose 5-phosphate (2-deoxyR5P) as an alternative substrate. Intriguingly, analysis of the specificity constants reveals that 2-deoxyR5P is a significantly better substrate than A5P for these active mutants than it is for wild-type enzymes. Indeed, for *Afe*KDO8PS, 2-deoxyR5P is as good a substrate for the N57A mutant as it is for the wild-type enzyme. This observation is completely consistent with an important role of this Asn in the KANRS motif for ensuring selection by these enzymes of the substrate with the correct stereochemistry (Figure 2).

PEP Binding Is Altered by Mutation of the Conserved Lys of the KANRS Motif. The Lys of the KANRS motif lies close to the PEP carboxylate binding site and may play a role in the binding of PEP; in *Aae*KDO8PS, this residue is observed to hydrogen bond to PEP, A5P, or both.[25] To assess the effect of the mutation of this residue, we studied PEP binding for both *Nme*K57A and *Afe*K55A by isothermal titration calorimetry (ITC). Weak binding of PEP to *Nme*K57A was observed, with a K_D value of 56 ± 14 μM (Figure S3 of the Supporting Information). Binding of a similar weak nature was observed for PEP with *Afe*K55A [K_D = 57.5 ± 0.6 μM (Figure S3 of the Supporting Information)]. These values are 10 times greater than those calculated when the same experiment was performed with the wild-type protein[26] (K_D^{Nme} = 4.8 ± 0.2 μM; K_D^{Afe} = 5.0 ± 0.1 μM), consistent with significant disruption to PEP binding upon mutation of this absolutely conserved Lys residue of the KANRS motif.

X-ray Crystal Structures. The crystal structure of wild-type *Nme*KDO8PS has previously been determined,[10] and similarly,

Table 3. Kinetic Parameters for 2-DeoxyR5P as an Alternate Aldose Substrate to A5P for Wild-Type *Nme*KDO8PS and *Afe*KDO8PS and Mutants *Nme*N59A and *Afe*N57A

	2-deoxyR5P			ratio of specificity constants[a]
	K_m	k_{cat} (s^{-1})	k_{cat}/K_m (s^{-1} mM^{-1})	A5P/2-deoxyR5P
wild-type *Nme*	230 ± 20 μM	0.13 ± 0.01	0.57 ± 0.09	1200
*Nme*N59A	432 ± 37 μM	0.0070 ± 0.0002	0.016 ± 0.002	18
wild-type *Afe*	5.0 ± 0.8 mM	0.66 ± 0.06	0.13 ± 0.03	1700
*Afe*N57A	1.5 ± 0.1 mM	0.202 ± 0.006	0.13 ± 0.01	28

[a] The ratio of specificity constants is k_{cat}/K_m for A5P divided by k_{cat}/K_m for 2-deoxyR5P.

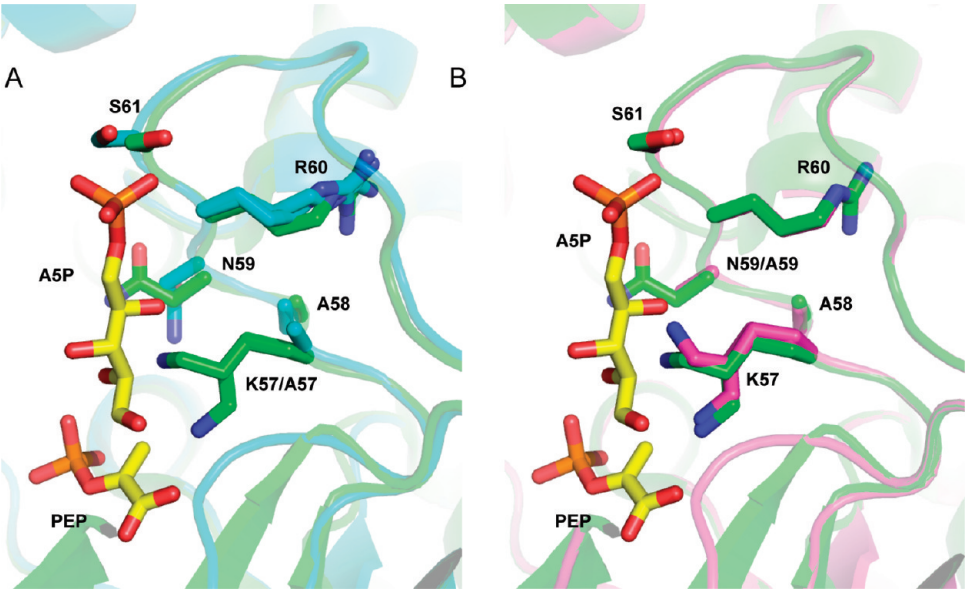

Figure 3. Overlay of the active sites of wild-type *Nme*KDO8PS (green), *Nme*K57A (cyan), and *Nme*N59A (magenta). (A) Wild type and *Nme*K57A. (B) Wild type and *Nme*N59A. Shown is chain C of each crystal structure. PEP and A5P are shown with carbon atoms colored yellow and positioned from an overlay of chain J of PDB entry 2NX3.[25] Lys57 is modeled in two alternative conformations in both wild-type KDO8P synthase and *Nme*N59A. Arg60 in *Nme*K57A is also modeled in two alternative conformations.

the structures of *Nme*K57A, *Nme*N59A, *Nme*KARS, and *Nme*KPRS feature one tetramer in each asymmetric unit. As expected, the construction of each subunit is unchanged in a $(\beta/\alpha)_8$ TIM-barrel topology. As in the wild-type structure, loops $\beta_7\alpha_7$ and $\beta_8\alpha_8$ are disordered, showing noncontinuous electron density. Loop $\beta_2\alpha_2$, on which the KANRS motif and these mutations are located, is well-defined in chains B and C and is moderately to poorly defined, in parts, in chains A and D. The *Nme*KARS mutant, in particular, shows noncontinuous electron density in these loops. Notwithstanding the lower resolution of the *Nme*KPRS data set, electron density maps were remarkably clean with the main chain and proline of the mutated region in the *Nme*KPRS mutant clearly defined and with the arginine side chain of the KPRS motif well-defined in three of the four chains.

For both *Nme*K57A and *Nme*N59A, the mutations are clearly visible. The only apparent change in the crystal structures is the respective truncation of the amino acid side chain. Few other changes are observed in the subunit structures (Figure 3), especially for the *Nme*N59A mutant, which superimposes very closely on the wild-type structure with an rmsd of 0.161 Å for superposition of Cα atoms of the tetrameric assembly. For the *Nme*K57A mutant, the corresponding rmsd is substantially greater (0.388 Å); the loss of the active-site lysine side chain leads to a slight repositioning of the $\beta_2\alpha_2$ loop bearing the K57A mutation in chains A, B, and D, as well as in chain D repositioning of the $\beta_1\alpha_1$ loop bearing the active-site Asn23 (to which Lys57 hydrogen bonds in the wild-type, *Nme*N59A, *Nme*KARS, and *Nme*KPRS structures).

In the structure of *Nme*KARS (rmsd for Cα atoms of 0.314 Å for superposition onto the wild-type structure), the shortening of the motif causes the backbone trace of the protein to take a shortcut (Figure 4). In chain A, the main chain shift is from Arg59 to Ile62 (from Arg60 to Ile63 in the wild type, respectively); the Cα of Arg59 is positioned approximately where that of Asn59 of the wild-type enzyme resided, and the side chain of Arg59 extends in the same direction as (and beyond that of) Asn59 to hydrogen bond with Gln117 of the adjacent subunit C. Ser60 and Ser61 occupy the positions of Arg60 and Ser61 in the wild-type structure, respectively. Register with the corresponding chain of the wild-type structure is not re-established until Ile62 (Ile63 in the wild type). The remainder of the $\beta_2\alpha_2$ loop is not observed in chain A (residues 63−68). In chains B and C, the main chain is shifted between Lys57 and Arg59 (exclusive), meaning that Ser60 and Ser61 are in positions similar to those of the wild-type enzyme (Ser61 and Ser62, respectively). The Cα atom of Arg59 in subunits B and C is positioned approximately in

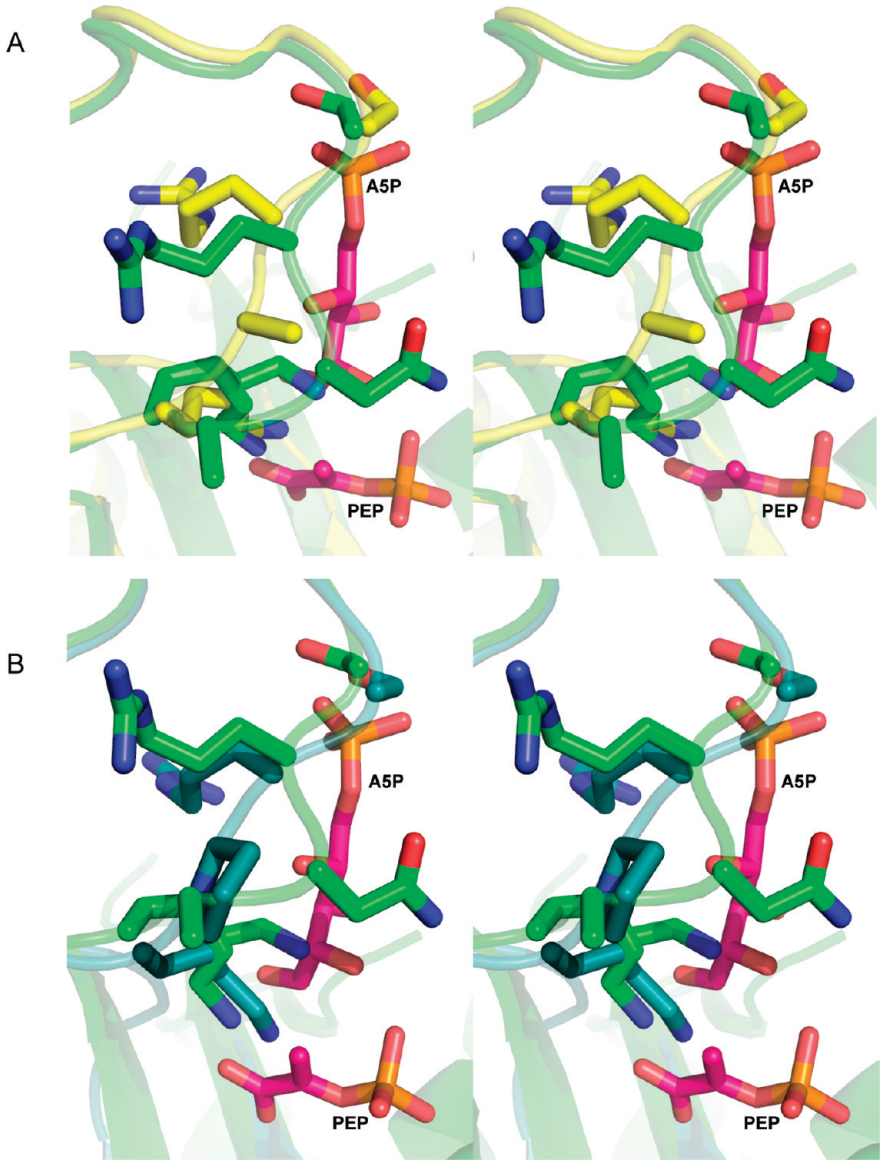

Figure 4. (A) Stereoview showing an overlay of chain C of *Nme*KARS (yellow) with wild-type *Nme*KDO8PS (green). (B) Stereoview showing an overlay of chain C of *Nme*KPRS (teal) with wild-type *Nme*KDO8PS (green). To indicate the substrate binding sites, PEP and A5P (magenta) are positioned from an overlay of chain J of PDB entry 2NX3.[25] The residues belonging to the native or mutated motif are shown as sticks.

place of that of Arg60 of the wild-type enzyme. However, unlike wild-type *Nme*KDO8PS where Arg60 projects into the interface with subunits D and A, forming an intersubunit salt bridge with Asp120 on loop $\beta_4\alpha_4$, in *Nme*KARS the side chain is oriented like that seen in the subunit of *Aae*KDO8PS that binds A5P (PDB entry 1FWW[12]). Chain D in this region is completely disordered, representing in extreme form the conformational plasticity of this $\beta_2\alpha_2$ loop.

In the structure of *Nme*KPRS, the backbone trace and the side chain conformations are similarly oriented and are very similar to those of *Nme*KARS, with the obvious exception of Pro58. In contrast to *Nme*KARS, the main chains of subunits A and D are defined for the $\beta_2\alpha_2$ loop, except that the side chain for Arg59 of chain A is not defined in electron density maps and Arg59 in chain D follows a trajectory similar to that in chain A of *Nme*KARS. The rmsd of the Cα atoms for superposition onto the wild-type structure is 0.294 Å.

DISCUSSION

Mutants of the conserved active-site KANRS motif in KDO8PS from *N. meningitidis* and *A. ferrooxidans* were successfully created, expressed, and purified. The purified proteins exhibited stability characteristics and overall structure similar to those of the wild-type proteins. The mutations did, however, affect the enzymic functioning. The notable feature of these analyses is that any mutation of this motif significantly prohibited both metal-dependent and metal-independent enzymes from playing their normal catalytic role.

Substitution of the KANRS Lys with Ala was completely deleterious for enzyme activity, and the role of this residue has never previously been directly probed in KDO8PS, despite being absolutely conserved and present in a key active-site location. The most recent structural analysis of both metal-dependent and metal-independent enzymes suggests that the amino functionality of this Lys is in the proximity of the A5P aldehydic

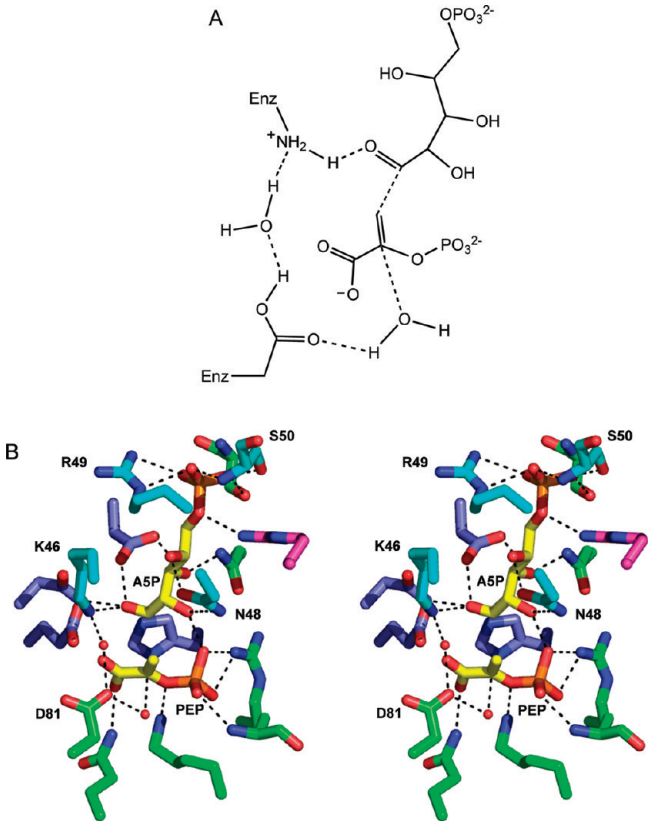

Figure 5. (A) Possible interactions involved in catalysis. (B) Stereodiagram of the interactions of the KANRS motif (cyan) with A5P (yellow), showing the role of Lys and Asn of the KANRS motif, chain J of PDB entry 2NX3.[25]

functionality. In this position, the aldehyde group is held in place by this Lys residue, and by coordination to the metal ion for metal-dependent KDO8PS, or by the Cys-substituted Asn for metal-independent KDO8PS.[27] This Lys clearly plays a role in the correct binding of A5P. The structure of the *Nme*KDO8PS K57A mutant suggests that the loss of the lysine side chain results in no significant structural change. Computational studies have suggested that the KDO8P synthase reaction proceeds by olefinic atom C3 of PEP attacking the aldehydic carbonyl. Protonation of the aldehydic carbonyl is required, and it appears likely that this Lys performs this critical catalytic role (Figure 5), either directly or via the nearby Asp residue that has also been shown to be essential.[10] Following attack by PEP on C1 of A5P, water is known to add to C2 of PEP, generating a linear tetrahedral diphosphate intermediate.[40] Computational studies have favored this water to approach from the *si* face of PEP giving an overall *syn* addition of A5P and water across the double bond of PEP.[27,41] However, it is apparent that the essential Lys of the KANRS motif links (via an absolutely conserved Asp, Asp92 in *Nme*KDO8PS and Asp81 in *Aae*KDO8PS) to a water molecule on the *re* face of PEP. This water molecule is observed and crystallographically conserved in most of the KDO8PS structures and is located ~2.8 Å from the olefinic moiety of PEP. This arrangement, and the importance of this Lys revealed by these studies, suggest that this *re* side water perhaps warrants further consideration, and that this residue may play a dual role in A5P binding and protonation. Attack by water in this arrangement would be in line with the proposed mechanisms for DAH7PS.[7,14]

In contrast to mutation of the Lys, mutation of the Asn residue of the KANRS motif to Ala did produce enzymes with some limited catalytic function. As the structure of the N59A mutant of *Nme*KDO8PS revealed no changes to the active site, this alteration in catalytic function is likely to be due to the loss of the amide side-chain functionality. These enzymes were substantially compromised in their ability to bind A5P but intriguingly were able to utilize 2-deoxyR5P, which is a poor alternative substrate for the wild-type enzymes, relatively well. For *Afe*KDO8PS, the N57A mutant was shown also to tolerate 2-deoxyR5P in a manner similar to that of the wild-type enzyme. Structures of substrate-bound *Aae*KDO8PS, mutated into a metal-independent form via replacement of the metal-binding Cys with Asn, show hydrogen bonding interactions between Asn of the KANRS motif and the hydroxyl groups that decorate A5P. With the carbonyl of A5P pointed toward the metal-binding site (or its equivalent in metal-independent enzymes), this Asn has been shown to hydrogen bond to the C2 hydroxyl group. The C2 hydroxyl group also forms a hydrogen bond with the phosphate group of PEP in these *Aae*KDO8PS mutants. The importance of these interactions for the reaction catalyzed by wild-type KDO8PS is revealed clearly by the observations that R5P with an altered C2 configuration is unable to act as an alternative substrate for the enzymes, and that 2-deoxyR5P (equivalent to 2-deoxyA5P) is an extremely poor substrate. The importance of the interaction between the C2 hydroxyl group of A5P and the wild-type enzyme is entirely consistent with the low activity of the Asn-to-Ala mutants (N59A and N57A), and the relative ambivalence of these mutants to the presence of the C2 hydroxyl group of A5P. Indeed, the low activity of both of these mutants mirrors, in part, the effects observed for the wild-type enzymes when the C2 hydroxyl group of A5P is removed. Interestingly, the metal-dependent enzymes are more tolerant of changes. 2-DeoxyR5P is a slightly better substrate for wild-type *Afe*KDO8PS than for the metal-independent *Nme*KDO8PS, and the N57A *Afe*KDO8PS mutant is slightly less compromised than the corresponding *Nme*KDO8PS mutant and notably demonstrates the same ability to utilize 2-deoxyR5P as wild-type *Afe*KDO8PS. This suggests that metal coordination plays a more prominent role in competent substrate binding than the equivalent amide functionality of the Asn residue that substitutes for the metal-binding Cys ligand to give the metal-independent enzymes. Mutation of Asn of the KANRS motif to Asp was lethal to activity. This observation is consistent with the inability of Asp, through the absence of a hydrogen bond donor, to perform a function similar to that of the Asn in this position.

Intriguingly, DAH7PS enzymes are far more tolerant of changes at C2 of the natural substrate E4P.[9] Indeed, the C2 configuration of E4P is the opposite to that of A5P. E4P is shorter with fewer degrees of freedom and therefore may not require the same anchoring that the A5P substrate requires to achieve reaction. DAH7PS enzymes are also more metal-dependent, and metal coordination may provide the key interaction that allows competent placement of substrate E4P for these enzymes.

Given the huge reduction in catalytic power upon the loss of the Asn of the KANRS motif, it is not surprising that the KARS and KPRS mutations exhibited no KDO8PS activity. As well as missing the key substrate binding contact with the Asn of the KANRS motif, as confirmed by the *Nme*KDO8PS structures of these mutants, the substrate-binding site has been shortened with the key phosphate binding Arg of the KANRS motif occupying a position similar to that of Asn59 in wild-type *Nme*KDO8PS. However, the change from KANRS to KPRS was not sufficient to

re-create DAH7PS activity, as these enzymes also did not utilize E4P. These results indicate very clearly that other features of the protein are important for supporting substrate selection and determining productive aldose phosphate binding.

While the KPRS motif is thought to be important for determining E4P selection in DAH7P synthases, analysis of both the sequences and structures of these enzymes indicates some of the features of KDO8P synthase that may preclude these *Nme*- and *Afe*KDO8PS mutants from utilizing E4P. There are other notable features that also may have a bearing on substrate selection in conjunction with the KPRS motif. The E4P/A5P binding site is situated close to the interface region between adjacent monomer units in the tetrameric enzyme. There are no interdigitating or shared residues between adjacent monomers in DAH7PS that might contribute directly to the active site. However, for KDO8PS, an Arg (R117 in *Nme*KDO8PS or R106 in *Aae*KDO8PS, which is part of a conserved PAFLXR motif in KDO8P synthase sequences) also makes contacts with the A5P phosphate. This Arg has been investigated previously in *Aae*KDO8PS and shown to be important for KDO8PS catalysis.[42] This residue provides a salt bridge to the A5P phosphate and facilitates closure of the $\beta_7\alpha_7$ loop (through precisely positioning the KANRS-containing $\beta_2\alpha_2$ loop). This Arg is still present in both the KPRS mutants, and its presence may discourage correct E4P binding. In contrast, DAH7P synthases provide Arg functionality to the aldose phosphate binding site from within the monomer unit, from the equivalent GARNXQ sequence motif. The $\beta_7\alpha_7$ loop that is closed on A5P binding is another obvious sequence and structural difference between the DAH7PS and KDO8PS. Assisted by the intersubunit Arg, this loop closes upon A5P binding.[42] Sequence alignments reveal that this $\beta_7\alpha_7$ loop is absent in DAH7P synthase.

In summary, these studies have shown that the KANRS motif is of prime importance to the function of KDO8P synthase. The Lys is critical, and this residue may act as a general acid in the reaction mechanism, thereby activating A5P directly to attack by cosubstrate PEP. The Asn of this motif appears to play an important role in the selection of the correct substrate by the enzyme. Simple conversion of this motif into the KPRS motif found absolutely conserved in the DAH7P synthases is not sufficient to switch substrate specificity from A5P to E4P, but this conversion is catastrophic for KDO8P synthase activity.

■ ASSOCIATED CONTENT

Supporting Information. Alignment of KDO8P synthase and DAH7P synthase sequences, melt temperatures of wild-type and mutant *Nme*KDO8PS and *Afe*KDO8PS in the presence of different divalent metal ions, circular dichroism spectra of wild-type and mutant *Afe*KDO8PS, subunit molecular weights of wild-type and mutant *Nme*KDO8PS and *Afe*KDO8PS as determined by time-of-flight liquid chromatography and mass spectrometry by ESI, and ITC data for the Asn-to-Ala mutations. This material is available free of charge via the Internet at http://pubs.acs.org.

■ AUTHOR INFORMATION

Corresponding Author

*Department of Chemistry, University of Canterbury, Private Bag 4800, Christchurch, New Zealand. Telephone: (+64) 3 364 5682. Fax: (+64) 3 364 2110. E-mail: emily.parker@canterbury.ac.nz.

Funding Sources

This research was funded, in part, by the New Zealand Marsden Fund (UOC0710), College of Science, University of Canterbury, through a Doctoral Scholarship for T.M.A., the Allan Wilson Centre for Molecular Ecology and Evolution for funding of the Rigaku MM007/RAxisIV^{++} X-ray generator and detector, and the Lottery Health Grants Board of New Zealand for funding the capillary optic at Massey University.

■ ACKNOWLEDGMENT

We thank Dr. Marie Squire for assistance with mass spectrometry. Part of this research was undertaken on the MX2 beamline at the Australian Synchrotron, Victoria, Australia.

■ ABBREVIATIONS

A5P, D-arabinose 5-phosphate; *Aae*, *Aq. aeolicus*; *Afe*, *A. thiobacilllus*; BTP, 1,3-bis[tris(hydroxymethyl)methylamino]propane; DAH7P, 3-deoxy-D-*arabino*-heptulosonate 7-phosphate; DAH7PS, 3-deoxy-D-*arabino*-heptulosonate 7-phosphate synthase; DSF, differential scanning fluorimetry; E4P, D-erythrose 4-phosphate; *Eco*, *E. coli*; IPTG, isopropyl β-D-thiogalactopyranoside; ITC, isothermal titration calorimetry; KDO, 3-deoxy-D-*manno*-octulosonate; KDO8P, 3-deoxy-D-*manno*-octulosonate 8-phosphate; KDO8PS, 3-deoxy-D-*manno*-octulosonate 8-phosphate synthase; LPS, lipopolysaccharide; *Nme*, *N. meningitidis*; PDB, Protein Data Bank; PEP, phosphoenolpyruvate; rmsd, root-mean-square deviation.

■ REFERENCES

(1) Levin, D. H., and Racker, E. (1959) Condensation of arabinose 5-phosphate and phosphoryl enol pyruvate by 2-keto-3-deoxy-8-phosphooctonic acid synthetase. *J. Biol. Chem. 234*, 2532–2539.

(2) Raetz, C. R. H., and Whitfield, C. (2002) Lipopolysaccharide endotoxins. *Annu. Rev. Biochem. 71*, 635–700.

(3) Wyckoff, T. J., Raetz, C. R., and Jackman, J. E. (1998) Antibacterial and anti-inflammatory agents that target endotoxin. *Trends Microbiol. 6*, 154–159.

(4) Bentley, R. (1990) The shikimate pathway: A metabolic tree with many branches. *Crit. Rev. Biochem. Mol. Biol. 25*, 307–384.

(5) Wagner, T., Kretsinger, R. H., Bauerle, R., and Tolbert, W. D. (2000) 3-Deoxy-D-*manno*-octulosonate-8-phosphate synthase from *Escherichia coli*. Model of binding of phosphoenolpyruvate and D-arabinose-5-phosphate. *J. Mol. Biol. 301*, 233–238.

(6) Shumilin, I. A., Kretsinger, R. H., and Bauerle, R. H. (1999) Crystal structure of phenylalanine-regulated 3-deoxy-D-*arabino*-heptulosonate-7-phosphate synthase from *Escherichia coli*. *Structure (Cambridge, MA, U.S.) 7*, 865–875.

(7) Shumilin, I. A., Bauerle, R., Wu, J., Woodard, R. W., and Kretsinger, R. H. (2004) Crystal structure of the reaction complex of 3-deoxy-D-*arabino*-heptulosonate-7-phosphate synthase from *Thermotoga maritima* refines the catalytic mechanism and indicates a new mechanism of allosteric regulation. *J. Mol. Biol. 341*, 455–466.

(8) Webby, C. J., Baker, H. M., Lott, J. S., Baker, E. N., and Parker, E. J. (2005) The structure of 3-deoxy-D-*arabino*-heptulosonate 7-phosphate synthase from *Mycobacterium tuberculosis* reveals a common catalytic scaffold and ancestry for type I and type II enzymes. *J. Mol. Biol. 354*, 927–939.

(9) Schofield, L. R., Anderson, B. F., Patchett, M. L., Norris, G. E., Jameson, G. B., and Parker, E. J. (2005) Substrate ambiguity and structure of *Pyrococcus furiosus* 3-deoxy-D-*arabino*-heptulosonate 7-phosphate synthase: An ancestral 3-deoxy-D-ald-2-ulosonate phosphate synthase?. *Biochemistry 44*, 11950–11962.

(10) Cochrane, F. C., Cookson, T. V. M., Jameson, G. B., and Parker, E. J. (2009) Reversing evolution: Re-establishing obligate metal ion

dependence in a metal-independent KDO8P synthase. *J. Mol. Biol. 390*, 646–661.

(11) Radaev, S., Dastidar, P., Patel, M., Woodard, R. W., and Gatti, D. L. (2000) Structure and mechanism of 3-deoxy-D-*manno*-octulosonate 8-phosphate synthase. *J. Biol. Chem. 275*, 9476–9484.

(12) Duewel, H. S., Radaev, S., Wang, J., Woodard, R. W., and Gatti, D. L. (2001) Substrate and metal complexes of 3-deoxy-D-*manno*-octulosonate-8-phosphate synthase from *Aquifex aeolicus* at 1.9 Å resolution. Implications for the condensation mechanism. *J. Biol. Chem. 276*, 8393–8402.

(13) Hartmann, M., Schneider, T. R., Pfeil, A., Heinrich, G., Lipscomb, W. N., and Braus, G. H. (2003) Evolution of feedback-inhibited β/α barrel isoenzymes by gene duplication and a single mutation. *Proc. Natl. Acad. Sci. U.S.A. 100*, 862–867.

(14) König, V., Pfeil, A., Braus, G. H., and Schneider, T. R. (2004) Substrate and metal complexes of 3-deoxy-D-*arabino*-heptulosonate-7-phosphate synthase from *Saccharomyces cerevisiae* provide new insights into the catalytic mechanism. *J. Mol. Biol. 337*, 675–690.

(15) Wu, J., and Woodard, R. W. (2006) New insights into the evolutionary links relating to the 3-deoxy-D-*arabino*-heptulosonate 7-phosphate synthase subfamilies. *J. Biol. Chem. 281*, 4042–4048.

(16) Webby, C. J., Jiao, W., Hutton, R. D., Blackmore, N. J., Baker, H. M., Baker, E. N., Jameson, G. B., and Parker, E. J. (2010) Synergistic allostery, a sophisticated regulatory network for the control of aromatic amino acid biosynthesis in *Mycobacterium tuberculosis*. *J. Biol. Chem. 285*, 30567–30576.

(17) Cross, P. J., Dobson, R. C., Patchett, M. L., and Parker, E. J. (2011) Tyrosine latching of a regulatory gate affords allosteric control of aromatic amino acid biosynthesis. *J. Biol. Chem. 286*, 10216–10224.

(18) Subramaniam, P. S., Xie, G., Xia, T., and Jensen, R. A. (1998) Substrate ambiguity of 3-deoxy-D-*manno*-octulosonate 8-phosphate synthase from *Neisseria gonorrhoeae* in the context of its membership in a protein family containing a subset of 3-deoxy-D-*arabino*-heptulosonate 7-phosphate synthases. *J. Bacteriol. 180*, 119–127.

(19) Jensen, R. A., Xie, G., Calhoun, D. H., and Bonner, C. A. (2002) The correct phylogenetic relationship of KdsA (3-deoxy-D-*manno*-octulosonate 8-phosphate synthase) with one of two independently evolved classes of AroA (3-deoxy-D-*arabino*-heptulosonate 7-phosphate synthase). *J. Mol. Evol. 54*, 416–423.

(20) Birck, M. R., and Woodard, R. W. (2001) *Aquifex aeolicus* 3-deoxy-D-*manno*-2-octulosonic acid 8-phosphate synthase: A new class of KDO 8-P synthase?. *J. Mol. Evol. 52*, 205–214.

(21) Duewel, H. S., and Woodard, R. W. (2000) A metal bridge between two enzyme families. 3-Deoxy-D-*manno*-octulosonate-8-phosphate synthase from *Aquifex aeolicus* requires a divalent metal for activity. *J. Biol. Chem. 275*, 22824–22831.

(22) Shulami, S., Furdui, C., Adir, N., Shoham, Y., Anderson, K. S., and Baasov, T. (2004) A reciprocal single mutation affects the metal requirement of 3-deoxy-D-*manno*-2-octulosonate-8-phosphate (KDO8P) synthases from *Aquifex pyrophilus* and *Escherichia coli*. *J. Biol. Chem. 279*, 45110–45120.

(23) Li, J., Wu, J., Fleischhacker, A. S., and Woodard, R. W. (2004) Conversion of *Aquifex aeolicus* 3-deoxy-D-*manno*-octulosonate 8-phosphate synthase, a metalloenzyme, into a nonmetalloenzyme. *J. Am. Chem. Soc. 126*, 7448–7449.

(24) Oliynyk, Z., Briseno-Roa, L., Janowitz, T., Sondergeld, P., and Fersht, A. R. (2004) Designing a metal-binding site in the scaffold of *Escherichia coli* KDO8PS. *Protein Eng., Des. Sel. 17*, 383–390.

(25) Kona, F., Xu, X., Martin, P., Kuzmic, P., and Gatti, D. L. (2007) Structural and mechanistic changes along an engineered path from metallo to nonmetallo 3-deoxy-D-*manno*-octulosonate 8-phosphate synthases. *Biochemistry 46*, 4532–4544.

(26) Allison, T. M., Yeoman, J. A., Hutton, R. D., Cochrane, F. C., Jameson, G. B., and Parker, E. J. (2010) Specificity and mutational analysis of the metal-dependent 3-deoxy-D-*manno*-octulosonate 8-phosphate synthase from *Acidithiobacillus ferrooxidans*. *Biochim. Biophys. Acta 1804*, 1526–1536.

(27) Tao, P., Schlegel, H. B., and Gatti, D. L. (2010) Common basis for the mechanism of metallo and non-metallo KDO8P synthases. *J. Inorg. Biochem. 104*, 1267–1275.

(28) Ahn, M., Pietersma, A. L., Schofield, L. R., and Parker, E. J. (2005) Mechanistic divergence of two closely related aldol-like enzyme-catalysed reactions. *Org. Biomol. Chem. 3*, 4046–4049.

(29) Gosset, G., Bonner, C. A., and Jensen, R. A. (2001) Microbial origin of plant-type 2-keto-3-deoxy-D-*arabino*-heptulosonate 7-phosphate synthases, exemplified by the chorismate- and tryptophan-regulated enzyme from *Xanthomonas campestris*. *J. Bacteriol. 183*, 4061–4070.

(30) Kohen, A., Berkovich, R., Belakhov, V., and Baasov, T. (1993) Stereochemistry of the KDO8P synthase. An efficient synthesis of the 3-fluoro analogs of KDO8P. *Bioorg. Med. Chem. Lett. 3*, 1577–1582.

(31) Kaustov, L., Kababya, S., Du, S., Baasov, T., Gropper, S., Shoham, Y., and Schmidt, A. (2000) Direct identification of enzyme active site residues by solid-state REDOR NMR: Application to KDO8P synthase. *J. Am. Chem. Soc. 122*, 2649–2650.

(32) Sheflyan, G. Y., Howe, D. L., Wilson, T. L., and Woodard, R. W. (1998) Enzymic synthesis of 3-deoxy-D-*manno*-octulosonate 8-phosphate, 3-deoxy-D-*altro*-octulosonate 8-phosphate, 3,5-dideoxy-D-*gluco*(*manno*)-octulosonate 8-phosphate by 3-deoxy-D-*arabino*-heptulosonate 7-phosphate synthase. *J. Am. Chem. Soc. 120*, 11027–11032.

(33) Ahn, M., Cochrane, F. C., Patchett, M. L., and Parker, E. J. (2008) Arabinose 5-phosphate analogues as mechanistic probes for *Neisseria meningitidis* 3-deoxy-D-*manno*-octulosonate 8-phosphate synthase. *Bioorg. Med. Chem. 16*, 9830–9836.

(34) Kohen, A., Jakob, A., and Baasov, T. (1992) Mechanistic studies of 3-deoxy-D-*manno*-2-octulosonate-8-phosphate synthase from *Escherichia coli*. *Eur. J. Biochem. 208*, 443–449.

(35) Ericsson, U. B., Hallberg, B. M., DeTitta, G. T., Dekker, N., and Nordlund, P. (2006) Thermofluor-based high-throughput stability optimization of proteins for structural studies. *Anal. Biochem. 357*, 289–298.

(36) Pflugrath, J. W. (1999) The finer things in X-ray diffraction data collection. *Acta Crystallogr. D55*, 1718–1725.

(37) Bailey, S. (1994) The CCP4 suite: Programs for protein crystallography. *Acta Crystallogr. D50*, 760–763.

(38) Murshudov, G. N., Vagin, A. A., and Dodson, E. J. (1997) Refinement of macromolecular structures by the maximum-likelihood method. *Acta Crystallogr. D53*, 240–255.

(39) Emsley, P., and Cowtan, K. (2004) Coot: Model-building tools for molecular graphics. *Acta Crystallogr. D60*, 2126–2132.

(40) Li, Z., Sau, A. K., Shen, S., Whitehouse, C., Baasov, T., and Anderson, K. S. (2003) A snapshot of enzyme catalysis using electrospray ionization mass spectrometry. *J. Am. Chem. Soc. 125*, 9938–9939.

(41) Tao, P., Gatti, D. L., and Schlegel, H. B. (2009) The energy landscape of 3-deoxy-D-*manno*-octulosonate 8-phosphate synthase. *Biochemistry 48*, 11706–11714.

(42) Xu, X., Kona, F., Wang, J., Lu, J., Stemmler, T., and Gatti, D. L. (2005) The catalytic and conformational cycle of *Aquifex aeolicus* KDO8P synthase: Role of the L7 loop. *Biochemistry 44*, 12434–12444.